Numerical Modelling of Creep Fracture Behaviour of Medium Density Polyethylene (MDPE)

I. Skozrit*, Z. Tonković
Faculty of Mechanical Engineering and Naval Architecture, University of Zagreb, Zagreb, Croatia

1. Abstract

The application of the reference stress method (RSM) to estimate the *J* and *C** integrals of cracked thick-walled metal as well as medium density polyethylene (MDPE) pipes is investigated. Unlike the existing solutions, the newly developed analytical approximations of the plastic limit pressure and *J*-integral are applicable to a wide range of crack dimensions in metal pipes. Based on the experimental data from literature and analogy between plasticity and creep, the paper discusses a method used to develop the efficient computational strategy for modeling creep fracture mechanisms by slow crack growth in a MDPE pipes.

2. Introduction

The increasing application of polymeric materials especial polyethylene's as structural materials demands new methodologies in order to assess the material capability to withstand loads. The use of MDPE pipes for water and gas distribution is one of the most common examples. An accurate modeling of fracture and viscoelastic material responses of such structures, represent a key for the prediction of structural integrity. Since the polyethylene structures are mostly subjected to creep loadings, the present paper is concerned with the numerical modeling of creep fracture mechanisms by slow crack growth in MDPE pipes [1]. The failure assessment philosophy for polymers is similar to philosophies for metals [2]. The *J*-integral equations can be used in principle to estimate the *C**-integral, by replacing strain with the strain rate [3]. In contrast to the internal axial semi-elliptical surface cracks [4, 5], a very limited number of studies have been reported in the area dealing with the determination of the *J*-integral and plastic limit load for metal pipes with external axial semi-elliptical surface cracks. The first part of the present contribution is concerned with the structural integrity of the metal thick-walled pipes subjected to internal pressure, having external axial surface cracks at the external wall. Based on the experimental data by Ben Hadj Hamouda et al. [6, 7] and analogy between plasticity and creep, the second part of the paper discusses a method used to develop the efficient computational strategy for modeling creep fracture mechanisms by slow crack growth in a MDPE pipes.

* Corresponding author. Tel.: +385 1 6168 115; fax: +385 1 6168 187.
E-mail address: ivica.skozrit@fsb.hr (Ivica Skozrit).

3. Reference stress based *J* estimation for surface cracked pipe

Finite element (FE) analysis has been performed to evaluate *J*-integral and plastic limit pressure for a thick-walled pipe with an external axial surface crack subjected to internal pressure. The pipe geometry and loading are shown in Fig. 1. R_i and R_o are the inner and the outer radius, while t denotes the wall thickness. The external surface crack is assumed to have a semi-elliptical shape described by a length $2c$ and depth a. Geometrically, an axial surface-cracked pipe is characterized by three non-dimensional parameters, i.e. R_i/t, c/a and a/t. As evident from Fig. 1, the internal pressure p is applied as a distributed load to the inner surface, together with an axial tension force F equivalent to the internal pressure applied at the end of the pipe to simulate the closed end. A parametric study is performed, in which an inner radius-to-thickness ratio R_i/t takes two values of 4 and 10. Thereat, the wall thickness of the pipe t is held constant at a value of 1.625 mm. These values are chosen to represent a standard thick-walled pipes geometry (mean radius-to-thickness ratio R_m/t typically less than 10). Four different half crack length-to-crack depth ratios of c/a = 5, 10, 15 and 20, and crack depth-to-thickness ratios of a/t = 0.2, 0.4, 0.6 and 0.8 are considered.
The finite element analysis is performed by using the commercial finite element package ABAQUS/Standard [8]. Twenty-noded isoparametric solid elements with reduced integration (C3D20R) are used to model the pipe. Due to symmetry, only a quarter of the pipe is modelled as shown in Fig. 2.

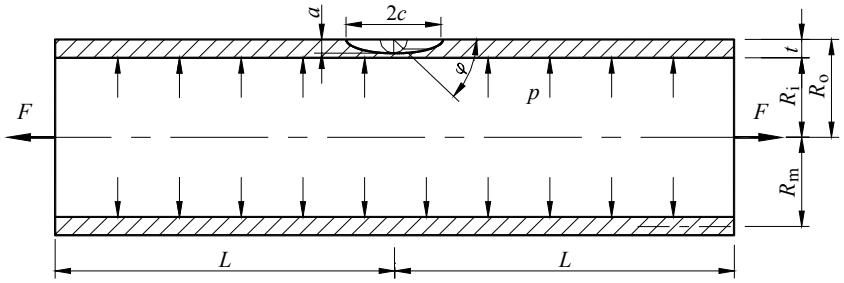

Figure 1 Geometry and dimensions of a pipe subjected to internal pressure.

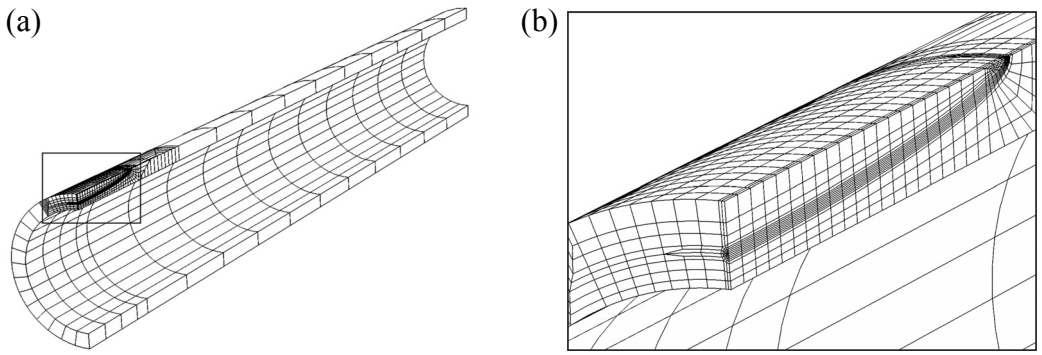

Figure 2 Typical FE mesh for a pipe: (a) whole mesh; (b) crack-tip mesh.

In the structural integrity assessment procedures the values of the elastoplastic J_{ep}-integral are obtained using the deformation theory of plasticity where the stress-strain response in the finite element analyses is described by the well-known Ramberg-Osgood model

$$\varepsilon / \varepsilon_0 = \sigma / \sigma_Y + \alpha(\sigma / \sigma_Y)^n . \quad (1)$$

In Eq. (1), σ_y is the yield stress, ε_0 denotes the associated reference strain $\varepsilon_0 = \sigma_Y / E$ and E is the Young's modulus. The values α and n represent the parameters fitting the experimentally obtained curve. With the method developed by the General Electric/Electric Power Research Institute (GE/EPRI), the total crack driving force J_{ep} can be split into elastic, J_{el}, and plastic, J_{pl}, parts, as

$$J_{ep} = J_{el} + J_{pl} \quad (2)$$

In the present investigation a total of 160 cases are considered to determine the J_{ep}-integral for external axial semi-elliptical surface cracks in thick pipes. Herein values of the strain hardening index n are systematically varied: n = 3, 5, 7 and 10, while parameter α is fixed to α = 1, where α and n represent the parameters fitting the experimentally obtained stress-strain curve. In addition, linear analyses with Poisson's ratio ν = 0.3 are performed to determine elastic component of J_{ep}, which is formulated according to [9]

$$J_{el}(\varphi) = (p \cdot R_m / t)^2 \pi \cdot a \cdot F^2 (R_m / t, a / t, c / a, \varphi) \quad (3)$$

where $F(R_m / t, a / t, c / a, \varphi)$ is a dimensionless function depending on the pipe and crack geometry and φ is the angle defining the crack front position (see Fig. 1). The values of function $F(R_m / t, a / t, c / a, \varphi)$ obtained from the FE analysis for the considered pipe geometry are tabulated in Table 1. As the J_{el} values reach the largest values at the deepest crack front location (φ = π/2), only the results at that location are given.

Table 1 Dimensionless function F for the stress intensity factor

R_m/t	4				10			
a/t	c/a				c/a			
	5	10	15	20	5	10	15	20
0.2	0.921	0.993	1.019	1.030	1.031	1.117	1.151	1.168
0.4	1.171	1.350	1.413	1.443	1.280	1.516	1.615	1.667
0.6	1.593	1.966	2.098	2.165	1.693	2.235	2.486	2.614
0.8	2.187	2.895	3.138	3.256	2.200	3.346	3.911	4.230

Following reference [4], the plastic part of J_{ep}-integral, J_{pl}, for semi-elliptical surface cracked pipes can be given by

$$J_{pl} = \alpha \sigma_y^2 / E (t - a) h_1 (R_m / t, a / t, c / a, \varphi) (p / p_L)^{n+1} \quad (4)$$

where σ_y is the yield stress and E denotes the Young's modulus. h_1 is the dimensionless plastic influence function which depends on the crack and pipe geometry, while p_L is the plastic limit pressure that produces the plastic collapse

of the surface cracked pipe for a rigid-plastic, non-hardening material with yield stress σ_y. Based on the finite element results, the empirical expression for the estimation of the plastic limit pressure p_L, in terms of the non-dimensional crack configuration parameters a/t and ρ is derived as follows:

$$p_L = p_0 \cdot P(a/t, \rho) \tag{5}$$

where p_0 is the limit pressure of an un-cracked thick-walled pipe based on the Von Mises yield criterion, $p_0 = 2/\sqrt{3}\sigma_y \ln(R_o/R_i)$, and ρ is normalized crack length defined as $\rho = c/\sqrt{R_m t}$ In Eq. 4, P is the dimensionless parameter which is a function of crack configuration parameters a/t and ρ, as follows:

$$P = 1 + P_1(a/t) + P_2(a/t)^2,$$
$$\text{where} \quad P_1 = 0.135312 - 0.351517 \cdot \rho + 0.067173 \cdot \rho^2 - 0.004954 \cdot \rho^3, \tag{6}$$
$$P_2 = 0.123488 - 0.011068 \cdot \rho + 0.009342 \cdot \rho^2 - 0.001921 \cdot \rho^3.$$

For the considered ranges, this empirical relation predicts the limit pressure which differs by less than 5% from values obtained by the finite element computation. Recently, Kim et al. [5] have proposed a similar equation for the plastic limit pressure based on selected FE limit analyses using the parameters $R_m/t = 20$, $\rho =$ 0.5, 1.0, 2.0 and 3.0. The plastic limit pressures for the considered pipe geometry obtained by the equation proposed by Kim et al. [5] are compared with the present FE results and Eq. 6 in Fig. 3. As may be seen, the finite element results presented in this work for the pipes with rather thick walls ($R_i/t = 4$) and large crack lengths are generally different from those obtained by [5]. These differences could arise from the fact that solutions obtained by [5] are given only for limited ranges of pipe and crack geometries.

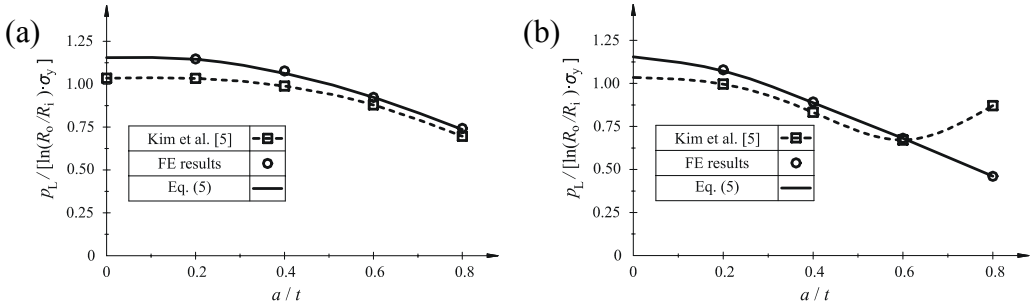

Figure 3 A comparison of plastic limit pressure p_L between the present work and the published solutions by Kim et al. [5] ($R_i/t = 4$): (a) $c/a = 5$; (b) $c/a = 20$.

In order to obtain the values of the function $h_1 = (R_m/t, a/t, c/a, \varphi)$ from Eq. 4, the plastic part of J_{ep} integral is determined by

$$J_{pl,FE} = J_{FE} - J_{el}. \tag{7}$$

It is to note that the value of h_1 depends on the load magnitude. Since the power-law part of the Ramberg-Osgood equation describing material behavior during the

loading process, is dominant at sufficiently large loads, the values of h_1 at high loads should be taken from appropriate diagrams. The values of h_1 for the considered pipe geometry at the deepest crack front location ($\varphi = \pi/2$) are presented in Table 2.

As presented in literature, the GE/EPRI results can be very sensitive due to the fitting of the stress-strain data when use the Ramberg-Osgood relation. For application to general stress-strain laws, the J_{ep} estimation equation is now re-formulated using the RSM [11]:

$$J_{ep} / J_{el} = E\varepsilon_{ref} / \sigma_{ref} + 0.5\left(\sigma_{ref} / \sigma_y\right)^2 \cdot \left(\sigma_{ref} / E\varepsilon_{ref}\right) \qquad (8)$$

where σ_{ref} denotes the reference stress, $\sigma_{ref} = \left(p / p_{ref}\right)\sigma_y$ and ε_{ref} is reference strain at $\sigma = \sigma_{ref}$, determined from the true-stress strain data, while p_{ref} stand for the reference pressure.

Table 2 Values of the plastic influence h_1-functions.

R_m/t	c/a	a/t	n				R_m/t	c/a	a/t	n			
			3	5	7	10				3	5	7	10
4	5	0.2	1.358	1.737	2.020	2.370	10	5	0.2	1.521	1.872	2.161	2.540
		0.4	5.563	7.228	8.357	9.482			0.4	6.424	8.254	9.739	11.386
		0.6	15.943	18.571	19.581	20.009			0.6	19.903	23.354	25.421	26.766
		0.8	37.093	38.727	38.132	34.822			0.8	51.712	57.183	60.255	59.333
	10	0.2	1.570	2.075	2.449	2.868		10	0.2	1.803	2.299	2.688	3.174
		0.4	6.556	8.604	9.708	10.356			0.4	8.395	11.071	12.818	14.223
		0.6	16.592	17.815	17.681	17.112			0.6	26.156	29.434	31.093	32.007
		0.8	29.855	27.973	25.438	21.583			0.8	57.742	58.603	60.943	60.396
	15	0.2	1.581	2.102	2.483	2.879		15	0.2	1.865	2.405	2.819	3.324
		0.4	6.312	8.256	9.146	9.504			0.4	8.678	11.579	13.262	14.492
		0.6	14.925	15.394	14.875	14.002			0.6	25.213	27.009	27.327	27.030
		0.8	27.514	27.749	27.309	25.622			0.8	47.198	45.301	45.762	43.527
	20	0.2	1.536	2.033	2.392	2.743		20	0.2	1.850	2.388	2.792	3.272
		0.4	5.958	7.772	8.554	8.803			0.4	8.387	11.241	12.750	13.676
		0.6	14.133	14.476	14.087	13.490			0.6	23.587	24.393	24.021	23.255
		0.8	22.731	22.968	22.615	21.040			0.8	43.821	42.614	44.701	45.104

Based on the FE results, the empirical expression for the estimation of the reference pressure p_{ref} in terms of non-dimensional crack configuration parameters a/t and ρ is derived

$$p_{ref} = \left(2/\sqrt{3}\right)\cdot\sigma_y \cdot \ln\left(R_o / R_i\right)\left[1 + A_1\left(a/t\right) + A_2\left(a/t\right)^2\right],$$

$$\text{where} \quad A_1 = -0.92351 - 0.18551\cdot\rho + 0.058677\cdot\rho^2 - 0.00539\cdot\rho^3, \qquad (9)$$

$$A_2 = 1.066525 - 0.16797\cdot\rho - 0.00265\cdot\rho^2 + 0.002479\cdot\rho^3.$$

The proposed Eq. 8 is compared with three-dimensional finite element results using actual experimental uniaxial stress-strain data of austenitic steel 08X18H10T [12] and incremental plasticity as well as GE/EPRI solutions. As

may be observed from Fig. 4, excellent agreement of the two RSM and FE solutions is exhibited. On the other hand, the results obtained by the GE/EPRI deviate significantly.

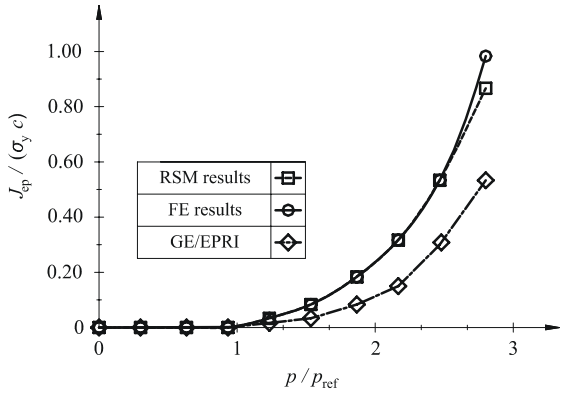

Figure 4 Comparison of FE and GE/EPRI *J* results with the proposed reference stress based *J* estimations $R_m/t = 4.8$, $c/a = 2.08$, $a/t = 0.8$.

4. *C**-integral estimation for MDPE

4.1. Analogy between plasticity and creep

In the previous section, an empirical expression for the estimation of the *J*-integral of cracked thick-walled pipes is proposed, based on the RSM. As presented in literature, at the sufficiently large load, Eq. 8 can be approximated as

$$J_{ep} = J_{el}\left(E\varepsilon_{ref} / \sigma_{ref}\right) \tag{10}$$

Based on the analogy between plasticity and creep, the C^*-integral for steady-state creep conditions is formulated using the RSM introduced by Ainsworth [11]

$$C^* = J_{el}\left(E\dot{\varepsilon}_c / \sigma_{ref}\right) \tag{11}$$

where $\dot{\varepsilon}_c$ is the creep strain rate at $\sigma = \sigma_{ref}$, determined from the actual creep-deformation data. Accordingly, an accurate modeling of nonlinear and time depended behavior of MDPE represent a key for the *C**-integral estimation.

4.2. Numerical modeling

The nonlinear time-dependent fracture behavior of MDPE has been investigated recently by Ben Hadj Hamouda et al. [6, 7] (Fig. 5). Creep cracking test has been performed on axisymmetrically cracked specimen denoted as full notched crack tensile (FNCT) and shown in Fig. 5b. As reported in [6, 7], the notch is made using a fresh razor blade with the crack tip radius approximately of 10 μm.

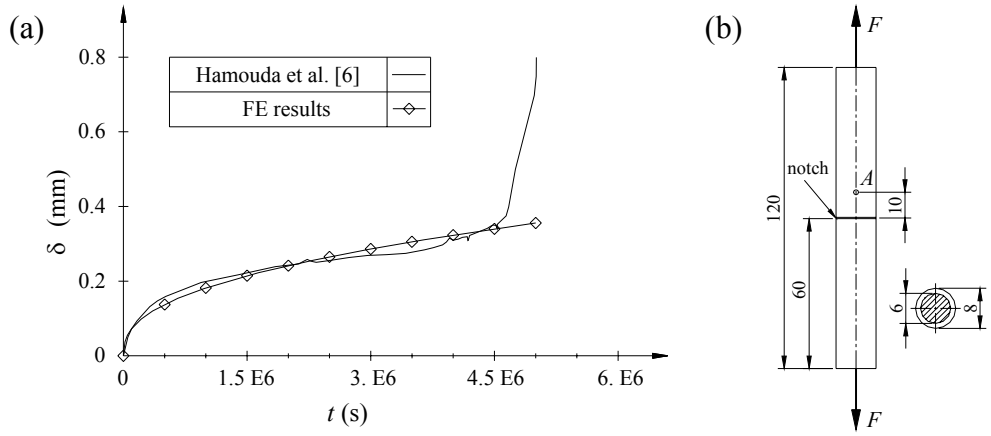

Figure 5 (a) Variation of creep displacement with time for a FNCT specimen at 60°C with $\sigma_{\text{net}} = 8\,\text{MPa}$ [6, 7], (b) full notched crack tensile (FNCT) specimen.

The experimental creep displacement δ versus time t diagram is obtained for a FNCT specimen tested at 60 ^{o}C under a net stress σ_{net} (load divided by the initial minimal cross-section) of 8 MPa (Fig. 5a). As may be observed from Fig. 5a, three stages can be distinguished in diagram. The primary creep stage (Stage I) is characterized by continuously decreasing of the displacement rate. During the Stage II constant displacement rate is obtained that corresponds to the stationary creep, while during Stage III crack accelerates and propagates through the remaining ligament until the ultimate fracture (tertiary creep).

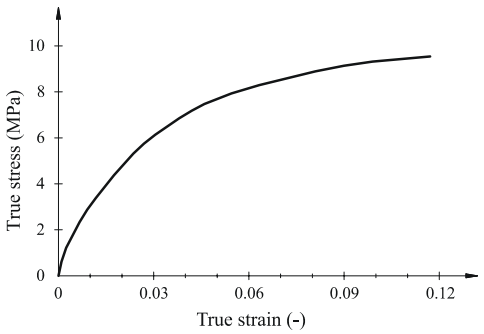

Figure 6 True stress-strain curve [6, 7].

Based on the above experimental results, the primary-secondary creep constitutive law is proposed as follows

$$\dot{\varepsilon}_{\text{c}} = B_1 p t^{(p-1)} \sigma^{n_1} + B_2 \sigma^{n_2} \tag{12}$$

where σ and ε_{c} are the stress and creep strain, while B_1, B_2, p, n_1 and n_2 stand for the material coefficients ($B_1 = 5.73 \cdot 10^{-9}$, $B_2 = 1.13 \cdot 10^{-12}$, $p = 0.41$, $n_1 = 5.81$ i $n_2 = 6.1$). In Eq. 12 dot designates derivative with time t. The first term on the right-hand side of Eq. 12 represents the primary creep and the second

term is the secondary portions of creep deformation. Fig. 6 displays the nonlinear elastic-plastic behavior of the considered MDPE in the form of the true stress-strain curve. The values of true terms are shown in Table 3.

Table 3 Material data of the MDPE.

True strain ε_t (-)	True stress σ_t (MPa)	True strain ε_t (-)	True stress σ_t (MPa)
0.00000	0.59	0.01595	5.38
0.00063	1.25	0.02666	6.73
0.00235	2.03	0.03349	7.37
0.00491	2.92	0.04506	8.05
0.00725	3.52	0.06392	8.77
0.00921	4.00	0.07856	9.19
0.01202	4.60	0.10283	9.54

The data is given up to the 11% of strain level. For the large strain FE analysis, after this specified point, the response is assumed to be perfectly plastic.

The main intention of the present work is to derive efficient computational strategy for modeling creep fracture mechanisms by slow crack growth in a MDPE, employing described material model. For power-law metal creep ABAQUS/Standard [8] provides an in-built routine for calculation of the C^*-integral. However, for generalized creep law, such as mentioned creep law for MDPE, calculation of the C^*-integral requires the user subroutine CREEP.

The implicit integration scheme is used to integrate the rate form of the constitutive model which leads to the following incremental form of the creep law defined by Eq. (12):

$$\varepsilon_{c,t+\Delta t} = \varepsilon_{c,t} + \Delta\varepsilon_c , \tag{13}$$

$$\Delta\varepsilon_c = B_1 \cdot \sigma^{n_1} \cdot \left[t^{p_1} - (t-\Delta t)^{p_1} \right] \text{ for } t \le t_{fp} , \tag{14}$$

$$\Delta\varepsilon_c = B_2 \cdot \sigma^{n_2} \cdot \Delta t \text{ for } t > t_{fp} , \tag{15}$$

where t_{fp} is transition time between primary and secondary creep. In the Eq. (13) the subscripts t and $t+\Delta t$ refer to the value of the creep strain at the beginning and at the end of the increment, respectively. Additionally, for the implicit integration algorithm the Jacobian matrix is derived and applied thereby:

$$\frac{\partial \Delta\varepsilon_c}{\partial \sigma} = \Delta\varepsilon_c \cdot \frac{n_1}{\sigma} \text{ for } t \le t_{fp} , \tag{16}$$

$$\frac{\partial \Delta\varepsilon_c}{\partial \sigma} = \Delta\varepsilon_c \cdot \frac{n_2}{\sigma} \text{ for } t > t_{fp} . \tag{17}$$

The computational strategy is based on the time hardening integration approach. The derived updating algorithm is implemented at the material point level of the available finite elements in the code ABAQUS [8] by using the user subroutine CREEP.

In order to check the accuracy of the algorithm derived, the creep simulation of FNCT specimen is performed. A typical finite element mesh for the FNCT specimen which will be applied in the analysis is shown in Fig. 7a. The mesh refinement in the vicinity of the blunted notch-tip is depicted in Fig. 7b. Employing symmetry, one quarter of the FNCT specimen section is modeled. For the model discretization, the eight-noded axisymmetric solid elements with reduced integration (CAX8R) are applied. The large strain FE model is employed by invoking the NLGEOM option within ABAQUS. A tension load is first applied to the FE model using a nonlinear elastic-plastic calculation at time $t = 0$. The load is then held constant and subsequent time-dependent creep analyses are performed. The creep displacement versus time curve, computed at the point A which is the exact location of the extensometer (see Fig. 5b), is compared with results of experimental investigations obtained in [6, 7]. As may be observed from Fig. 5a, the finite element results correspond well with the experimental results.

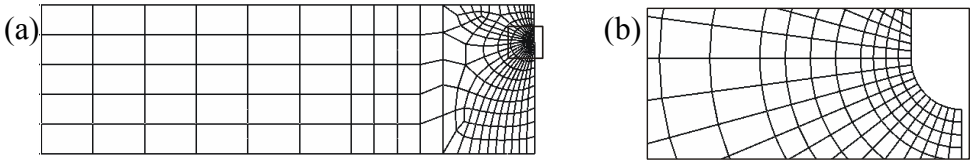

Figure 7 Typical finite element mesh for FNCT specimen: (a) whole mesh; (b) notch-tip mesh.

Currently we are working on the systematic detailed non-linear finite element analyses to determine the C^*-integral for the presented FNCT specimen as well as a thick-walled MDPE pipe with an external axial surface crack subjected to internal pressure.

5. Conclusion

The application of the reference stress method to estimate the J-integral of cracked thick-walled metal pipes is presented. It is shown that, compared to existing solutions, the newly developed analytical approximations of the plastic limit pressure and J-integral are applicable to a wide range of crack dimensions. Based on the experimental data from literature and analogy between plasticity and creep, the paper discusses a method used to develop the efficient computational strategy for modeling creep fracture mechanisms by slow crack growth in a MDPE pipes which will be considered in the further work. Systematic detailed non-linear finite element analyses will be carried out to determine the C-integral as a function of time for a thick-walled MDPE pipe with an external axial surface crack subjected to internal pressure.

References

[1] X. Lu, N. Brown, The transition from ductile to slow crack growth failure in a copolymer of polyethylene, Journal of Materials Science 25 (1990) 411–416

[2] E. Krempl, F. Kahn, Rate (time)-dependent deformation behavior: an overview of some properties of metals and solid polymers, International Journal of Plasticity 19 (2003) 1069-1095

[3] Y.-J. Kim, J.-S. Kim, N.-S. Huh, Y.-J. Kim, Engineering C-integral estimates for generalised creep behaviour and finite element validation, International Journal of Pressure Vessels and Piping 79 (2002) 427–443

[4] Y.-J. Kim, J.-S. Kim, Y.-J. Park, Y.-J. Kim, Elastic-plastic fracture mechanics method for finite internal axial surface cracks in cylinders, Engineering Fracture Mechanics 71 (2004) 925-944

[5] Y.-J. Kim, D.-J. Shim, K. Nikbin, Y.-J. Kim, S.-S. Hwang, J.-S. Kim, Finite element based plastic limit loads for cylinders with part-through surface cracks under combined loading, International Journal of Pressure Vessels and Piping 80 (2003) 527-540

[6] H.B.H. Hamouda, L. Laiarinandrasana, R. Piques, Fracture mechanics global approach concepts applied to creep slow crack growth in a medium density polyethylene (MDPE), Engineering Fracture Mechanics 74 (2007) 2187-2204

[7] H.B.H. Hamouda, L. Laiarinandrasana, R. Piques, Viscoplastic behaviour of a medium density polyethylene (MDPE): Constitutive equations based on double nonlinear deformation model, International Journal of Plasticity 23 (2007) 1307-1327.

[8] ABAQUS/Standard, User's guide and theoretical manual, Version 6.8, Hibbitt, Karlsson & Serensen, Inc. (2008).

[9] I.S. Raju, J.C. Newman, Stress-intensity factors for internal and external surface cracks in cylindrical vessels, Journal of Pressure Vessel Technology 104 (1982) 293–298

[10] Z. Tonković, I. Skozrit, J. Sorić, Numerical modelling of deformation responses of cracked tubes, Transactions of FAMENA 29 (2005) 31-38

[11] R.A. Ainsworth, The assessment of defects in structures of strain hardening material, Engineering Fracture Mechanics 19 (1984) 633–642

[12] Z. Tonković, I. Skozrit, I. Alfirević, Influence of flow stress choice on the plastic collapse estimation of axially cracked steam generator tubes, Nuclear Engineering and Design 238 (2008) 1762-1770